Cellular Physiology and Biochemistry

Cell Physiol Biochem 2018;45:917-934
DOI: 10.1159/000487286
Published online: February 08, 2018
Accepted: January 09, 2018

Original Paper

ITRAQ-Based Proteomics Analysis of Triptolide On Human A549 Lung Adenocarcinoma Cells

Fangqiong Li[a] Dongxiao Zhao[a] Suwen Yang[b] Juan Wang[a] Qin Liu[a] Xin Jin[a] Wei Wang[a]

[a]Department of Clinical Laboratory, Tongde Hospital of Zhejiang Province, Hangzhou, [b]Department of Clinical Laboratory, Sir Run Run Shaw Hospital, Medical College, Zhejiang University, Hangzhou, P.R. China

Key Words

Triptolide • NSCLC • ITRAQ • Proteome

Abstract

Background/Aims: Triptolide (TP) is a diterpenoid triepoxide extracted from the traditional Chinese medical herb *Tripterygium wilfordii* that exerts prominent broad-spectrum anticancer activity to repress proliferation and induce cancer cell apoptosis through various molecular pathways. We previously observed that TP inhibits the progression of A549 cells and pancreatic cancer cells (PNCA-1) *in vitro*. However, the complex molecular mechanism underlying the anticancer activity of TP is not well understood. ***Methods:*** To explore the molecular mechanisms by which TP induces lung cancer cell apoptosis, we investigated changes in the protein profile of A549 cells treated with TP using a proteomics approach (iTRAQ [isobaric tags for relative and absolute quantitation] combined with NanoLC-MS/MS [nano liquid chromatography-mass spectrometry]). Changes in the profiles of the expressed proteins were analyzed using the bioinformatics tools OmicsBean and the Kyoto Encyclopedia of Genes and Genomes (KEGG) and were verified using western blotting. Apoptosis and cell cycle effects were analyzed using flow cytometry. ***Results:*** TP induced apoptosis in A549 cells and blocked A549 cells at the G2/M phase. Using iTRAQ technology, we observed 312 differentially expressed proteins associated in networks and implicated in different KEGG pathways. Gene Ontology (GO) analysis showed the overviews of dysregulated proteins in the biological process (BP), cell component (CC), and molecular function (MF) categories. Moreover, some candidate proteins involved in PARP1/AIF and nuclear Akt signaling pathways or metastasis processes were validated by western blotting. ***Conclusion:*** TP exerted anti-tumor activity on non-small cell lung cancer (NSCLC) A549 lung adenocarcinoma cells by dysregulating tumor-related protein expression. Herein, we provide a preliminary study of TP-related cytotoxicity on A549 cells using proteomics tools. These findings may improve the current understanding of the anti-tumor effects of TP on lung cancer cells and may reveal candidate proteins as potential targets for the treatment of lung cancer.

Wei Wang

Department of Clinical Laboratory, Tongde Hospital of Zhejiang Province
No. 234 Gucui Road, Hangzhou, Zhejiang 310012 (China)
Tel. +86-0571-89972216, Fax +86-0571-89972216, E-Mail wangweihz8@163.com.cn

Introduction

Lung cancer is one of the most prevalent malignancies in humans, and its incidence and mortality are increasing worldwide [1]. Approximately 80% of lung cancers are non-small cell lung cancers (NSCLCs). Although diagnostic and treatment methods have recently improved markedly, no significant improvements in the prognosis of patients with NSCLC have been achieved, as the 5-year survival rates for all patients diagnosed with lung cancer remain at approximately 15% [2, 3]. Currently, the major methods for lung cancer treatment include surgery, chemotherapy and radiotherapy. Among these methods, chemotherapy can significantly relieve symptoms and improve patient quality of life. However, the efficacy and safety of this treatment remain a primary concern. Chemotherapy drugs have some serious side effects, and the toxicity of these drugs has always been an obstacle to clinical applications [4]. Therefore, the development of new therapeutic drugs for lung cancer that have high efficacy and low toxicity is clinically important.

Triptolide (TP), originally extracted from the traditional Chinese medicinal plant *Tripterygium wilfordii* [5], has been confirmed to have myriad biological properties, including immunosuppression and anti-inflammatory effects, and has been applied for the treatment of autoimmune diseases, such as nephritis and rheumatoid arthritis [6-8]. Recently, numerous studies have demonstrated that TP possesses prominent anti-tumor activities in diverse tumor cell types *in vitro*, such as breast [9], pancreatic [10], ovarian [11], lung [12], and prostate cancers [13]. TP can also prevent tumor growth *in vivo* via cell proliferation inhibition and apoptosis induction [14]. Moreover, studies have reported that TP sensitizes human cancer cells to cisplatin, 5-fluorouracil (5-FU) and TNF-alpha-induced apoptosis *in vivo* and *in vitro* [15, 16]. In a previous study, we observed that TP induces apoptosis in human lung cancer cells through PP2A-regulated ERK, p38, MAPK and Akt signaling pathways [17]. Until recently, the activity of TP in inducing tumor cell death has been well documented, but the complex molecular targets of TP anti-tumor activity have not been well characterized. Thus, a powerful tool to accurately monitor and quantitatively detect changes in protein expression in response to TP treatment is needed.

Proteomics approaches, enabling relatively comprehensive global analyses, have been widely used to examine complex biological functions [18-20]. The isobaric tags for the relative and absolute quantitation (iTRAQ) method combined with nano liquid chromatography-mass spectrometry (NanoLC-MS/MS), developed for protein quantitation, represent a high-throughput quantitative technique with high sensitivity and reproducibility. Currently, iTRAQ-based proteomics has been widely used to investigate the mechanistic effects of chemicals on cancer [21-24].

In the present study, we employed a strategy combining iTRAQ with NanoLC-MS/MS to analyze alterations in the protein profile of the A549 lung adenosquamous carcinoma cell line following TP treatment. Differential protein expression data may provide a valuable resource to reveal potential molecular targets underlying the anticancer activity of TP and to improve the understanding of the anti-tumor effects of TP on lung cancer.

Materials and Methods

Cell culture and treatment

Human lung cancer A549 cells (American Type Culture Collection; ATCC CCL185) were maintained in monolayer culture at 37°C in a humidified atmosphere with 5% CO_2 in RPMI-1640 medium (Gibco-BRL, USA) supplemented with 10% fetal bovine serum (FBS) (Sijiqin Biotechnology Co. Ltd., China) and 1% penicillin/streptomycin solution (100 U/ml penicillin and 100 μg/ml streptomycin). A total of 20 mg of TP (purity≥98%, Beijing Fan-China Biotechnology Co., Ltd.) was dissolved in 0.5 ml dimethylsulfoxide (DMSO) to obtain a 100% stock solution, which was subsequently stored at -20°C and diluted with medium prior to use in experiments. The final DMSO concentration did not exceed 0.1% (v/v) throughout the study. For

exposure experiments, A549 cells at approximately 80% confluency were transferred to medium containing 12.5, 50, and 200 ng/ml of TP and were cultured for 36 h (24-h 50% inhibitory concentration [IC50]=273.0 ng/ml) [17]. Cells treated with an equal amount of DMSO were employed as a control, and all of the treatments were performed in triplicate. Three replicate proteomics analyses were performed for each test concentration and the control group. The iTRAQ experimental results described herein are only for the 200 ng/ml TP concentration, as cells represented more acute TP cytotoxicity at this concentration.

Flow cytometric cell cycle and cell apoptosis analysis

The effects of TP on cell cycle progression were measured using flow cytometry. The fixed cells were stained with propidium iodide (PI, ComWin Biotech Co. Ltd., China) solution (50 μg/ml PI and 100 μg/ml RNase A in PBS) and were subsequently subjected to cell cycle analysis. Cell apoptosis was measured using Annexin V/PI double staining (ComWin Biotech Co. Ltd., China). Briefly, 100 μl of binding buffer containing 2.5 μl of Annexin V-fluorescein isothiocyanate (FITC) and 1 μl of PI was added to the cell suspension, followed by incubation for 30 min in the dark. The samples were assayed using a Beckman-Coulter Flow Cytometer with excitation at 488 nm and emission at 525 nm for FITC and 575 nm for PI. The data were analyzed using FlowJo software.

Protein preparation

The harvested cells were washed five times using ice-cold PBS and disrupted using enhanced RIPA lysis buffer (Beyotime Co., China) containing protease and phosphatase inhibitors for 30 min on ice, followed by ten cycles of 5-second bursts of sonication with 30-second intervals. The cell debris was removed by centrifugation at 12, 000×g for 30 min at 4°C, and the supernatants were collected. Protein concentrations were assayed using a bicinchoninic acid (BCA) protein assay kit according to the manufacturer's instructions (Beyotime Co., China). Bovine serum albumin (BSA) was used as the standard.

iTRAQ labeling and high-pH RPLC fractionation

The iTRAQ Reagent 4-Plex kit (AB Sciex, USA) was used according to the manufacturer's instructions to label peptides. Equal amounts of protein (100 μg per sample) obtained from TP-treated and control cells were labeled using iTRAQ labeling reagents. The TP-treated samples were labeled using 117, while the control samples were labeled using 114. Briefly, the proteins in each sample were reduced with dithiothreitol (DTT) and were subsequently alkylated with iodoacetamide. The samples were digested overnight at 37°C using trypsin (AB Sciex, USA) at a trypsin:protein ratio of 1:20 (W/W). The tryptic peptides were labeled using iTRAQ reagents. The labeled samples were combined and lyophilized. The peptide mixtures were dissolved in high-pH reverse phase (HP-RP) solvent A (20 mM ammonium formate, pH 10.0). The peptides were fractionated using the Shimadzu LC-30A system with a Durashell-C18 column (4.6 mm×250 mm, 5 μm 100 Å, Agela, China) for high-pH RP chromatography. A total of 40 RP fractions were collected and subsequently dried and reconstituted using 30 μl of 0.1% FA for NanoLC-MS/MS analysis.

NanoLC-MS/MS analysis

Separation was performed using the Eksigent nanoLC-Ultra™ 2D System combined with the cHiPLC™-Nanoflex system in Trap-Elute mode connected to a Triple TOF 4600 mass spectrometer (AB Sciex, USA). Briefly, 8 μl of each fraction was loaded onto the cHiPLC trap (200 μm × 500 μm ChromXP C18-CL 3 μm 300 Å) and washed for 15 min at 2 μl/min. Subsequently, an elution gradient of 10-43% acetonitrile (0.1% formic acid) in an 85-min gradient at 300 nl/min was used on a nano cHiPLC column (75 μm × 15 cm ChromXP C18-CL 3 μm 300 Å). The MS analysis was performed using a nano ion spray voltage maintained at 2.3 kV and a scan range of 350 to 1500 (m/z) in the positive-ion mode. Full-scan MS spectra were acquired from 40 precursors selected for MS/MS from an m/z 100-1500 range using a dynamic exclusion setting of 30 s. The IDA CE parameter script, which selected up to 40 precursors with charge states of 2+ to 4+, automatically controlled the collision energy (CE). The mass spectrometer was calibrated using the tryptic peptides of beta-galactosidase.

Protein identification and quantitation

Peptide identification and quantification were conducted using ProteinPilot 4.2 software (AB Sciex, USA). The following search parameters were used: (1) sample type, iTRAQ 4-plex (Peptide Labeled); (2)

cysteine alkylation, iodoacetamide; (3) digestion, trypsin; (4) instrument, Triple TOF 4600; (5) special factors, none; (6) species, Homo sapiens; (7) ID Focus, biological modifications; (8) database, UniProtKB/Swiss-Prot FASTA; and (9) search effort, Thorough ID. In the iTRAQ quantitation, the Pro Group algorithm was automatically selected to calculate the reporter-peak areas. To estimate the false discovery rate (FDR) for peptide identification, a decoy database search strategy was adopted. For this study, a strict unused confidence score of >1.3 was used as the qualification criterion, corresponding to a peptide confidence level of 95%. If the iTRAQ ratios were >2.0 or <0.5 in the samples obtained from the TP-treated A549 cells relative to those of the control group, then the proteins were considered differentially expressed.

Bioinformatics analysis of proteomics data

The identified proteins were classified according to annotations from the UniProt knowledge base (Swissprot/TrEMBL, http://www.uniprot.org/).The multi-omics data analysis tool, OmicsBean, was used to analyze the obtained proteomics data (http://www.omicsbean.com), in which distributions in biological process (BP), cellular components (CCs) and molecular functions (MF) were assigned to each protein based on Gene Ontology (GO) categories. Kyoto Encyclopedia of Genes and Genomes (KEGG) pathway analysis (http://www.genome.ad.jpkegg/pathway.html) was performed to enrich high-level functions in the defined biological systems. Protein-protein interaction (PPI) analysis was performed using Cytoscape software, with a confidence cutoff of 400; interactions with larger confident scores are indicated with solid lines between genes/proteins, or otherwise shown as dashed lines.

Western blotting

The A549 cells were washed twice with cold PBS and lysed in 200 μl RIPA lysis buffer (50 mM Tris-HCl, 150 mM NaCl, 1% Triton X-100, 1% sodium deoxycholate, and 0.1% sodium dodecyl sulfate; Beyotime Co., China) containing 100 mM phenylmethanesulfonyl fluoride (PMSF; Beyotime Co., China) for 30 min on ice. The lysates were centrifuged at 14, 000×g for 10 min at 4°C, and the supernatants were collected. Twenty micrograms of protein/well was loaded onto 10% gels for separation using sodium dodecyl sulfate-polyacrylamide gels electrophoresis (SDS-PAGE). The gels were electrophoretically transferred onto polyvinylidene fluoride (PVDF) membranes (0.45 or 0.20 μm pore size; Millipore, Billerica, MA, USA). The blotted membranes were blocked with 5% nonfat dry milk in a Tris-buffered saline solution (25 mM Tris, pH 7.5, and 150 mM NaCl) containing 0.05% Tween 20 (TBST) for 2 h at room temperature, followed by incubation with the diluted primary antibody against target protein for 4 h at room temperature. After washing for 10 min in TBST solution, the membranes were incubated with properly diluted secondary antibody conjugated with horseradish peroxidase for 2 h at room temperature. Western signals were developed using ECL chemiluminescent reagents from Thermo Scientific (Waltham, MA, USA). The β-actin levels were used as loading controls.

Statistical analysis

Western blotting and flow cytometry results are presented as the means ± standard deviations (SD) from three independent experiments. Statistical analysis of the quantitative data for multiple group comparisons was performed using one-way ANOVA. Duncan's test (two sided) was used to determine the statistical significance levels ($P<0.05$ and $P<0.01$) between control and TP-treated groups.

Results

TP-induced apoptosis of A549 cells

To investigate the effects of TP on apoptosis in A549 cells, Annexin V/PI staining-based FACS analysis was performed to detect the externalization of phosphatidylserine on the cell membrane, a hallmark of early apoptosis. Cells undergoing early-stage apoptosis were stained with Annexin V-FITC+/PI-, and late apoptotic cells were stained with Annexin V+/PI+. Fig. 1A quantifies the increase in early apoptotic cells labeled with Annexin V+/PI-, showing increases from 3.2% in the control group to 14.8, 20.4% and 27.3% in the TP-treated groups, respectively. In addition, the overall apoptotic rates were significantly increased in the TP groups. These findings revealed that various TP treatments induced significantly higher

percentages of apoptotic cells than the control group (Fig. 1B), indicating that TP can promote apoptosis.

Effects of TP on cell cycle arrest

The effects of TP on the cell cycle are shown in Fig. 2. Compared with the control group, the percentage of cells in the G0/G1 phase decreased from 63.84% to 13.75%, whereas the percentage of cells in the G2/M phase increased from 14.66% to 64.56%. These results indicated that TP blocks A549 cells at the G2/M phase.

Comparative proteomics of TP-treated A549 cells versus control A549 Cells

The proteins were extracted from cells treated in parallel. The samples were digested using trypsin and were labeled using 114 and 117 iTRAQ tags, and the labeled digests were utilized for MS analysis (Fig. 3A). The database we searched contains 376809 entries. Using ProteinPilot 4.5, we identified totals of 4977/5102/4762 proteins in these two cell lines in the three runs (Local FDR of <5%). Using filters with an unused protein score of >1.3 and a number of peptides of ≥2, 4561/4446/4302 proteins were identified (Table 1). In total, we identified 141 up-regulated (with 117:114 iTRAQ ratios of >2.0) and 171 down-regulated proteins (with 117:114 iTRAQ ratios of <0.5) in TP-treated A549 cells compared with

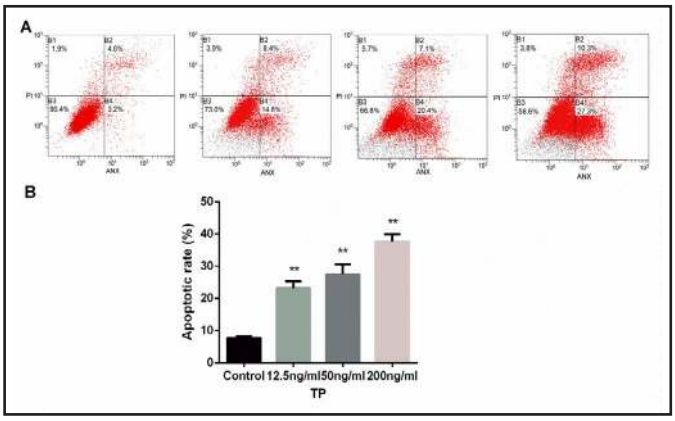

Fig. 1. Apoptotic effects of TP on human lung cancer A549 cells. (A) After 36 h of TP treatment (12.5, 50, and 200 ng/ml), A549 cells were stained with Annexin V-FITC and PI and analyzed using flow cytometry. Early apoptotic cells were Annexin V+/PI–, and late apoptotic cells were Annexin V+/PI+. (B) The overall apoptotic rates were significantly increased after TP treatment. **P<0.01 compared with the control group. Data are presented as the means ± SD of three independent experiments.

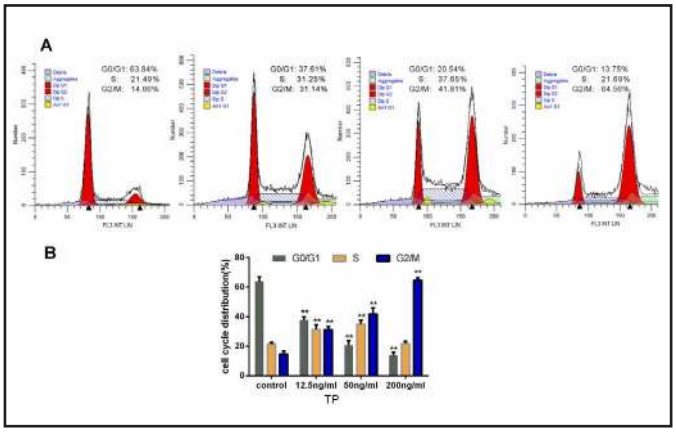

Fig. 2. Effects of TP on cell cycle distribution in human lung cancer A549 cells. (A) Representative histograms depicting cell cycle distributions in A549 cells treated with TP. After 36 h of TP exposure (0, 12.5, 50 and 200 ng/ml), A549 cells were stained with PI and analyzed using flow cytometry. (B) The percentage of the total cell population in each phase of the cell cycle is represented as a bar diagram. **P<0.01 compared with the control group. Data are presented as the means ± SD of three independent experiments.

Table 1. Summarized results of three iTRAQ experiments

Experiment No.	Number of distinct proteins Local FDR (<5%)	Number of distinct peptides Local FDR (<5%)	Number of spectra Local FDR (<1%)	Unused protein score(>1.3) and peptide(>2)
1	4977	57223	17567	4561
2	5102	60205	17634	4446
3	4762	56342	16589	4302

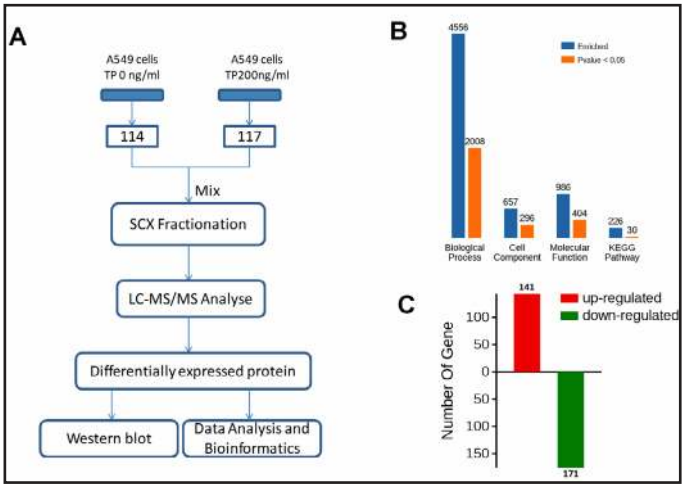

Fig. 3. Experimental quantitative proteomics analysis workflow and results. (A) Experimental design for the quantitative proteomics analysis. The proteins from A549 cells treated with different concentrations of TP were digested with trypsin and labeled using 114/117/iTRAQ tags. The labeled digests were analyzed using Nano LC-MS/MS. The differentially expressed proteins were evaluated using western blotting and analyzed through database searches. (B) The enriched counts for Biological Process, Cellular Component, Molecule Function, and KEGG Pathway. The counts for each category represent the total number of terms in the database associated with the query gene/protein list. Terms with P-values<0.05 are statistically significant. (C) In total, 312 proteins were identified, including 141 up-regulated proteins and 171 down-regulated proteins.

the control cells (Fig. 3C, Tables 2 and 3). Among those 312 dysregulated proteins, 50 proteins related to cell apoptosis were enriched (Table 4) . Afterward, we performed a cluster analysis to get the heatmap which contains the data obtained for the 312 dysregulated proteins. The three horizontal clusters represent the technical replicates (Fig. 4).

Functional enrichment of the TP-regulated proteins

The obtained protein data were analyzed using bioinformatics approaches to extract information relevant to the involved pathways. Enrichments of TP-related proteins in BP, CC, and MF categories based on GO analysis are shown in Fig. 3B. In the BP analysis, the majority of identified proteins were classified into metabolic processes, particularly nitrogen compound metabolism and cellular nitrogen compound metabolism. The CC analysis showed that most of the identified proteins belonged to organelles and membrane-bounded organelles. The molecular functional classification revealed that most of these proteins were involved in binding, heterocyclic compound binding, and protein binding (Fig. 5.). GO analysis indicated that these TP-induced differentially expressed proteins exhibited a wide variety of cellular distributions and functions, consistent with the fact that TP has broad-spectrum anti-tumor effects.

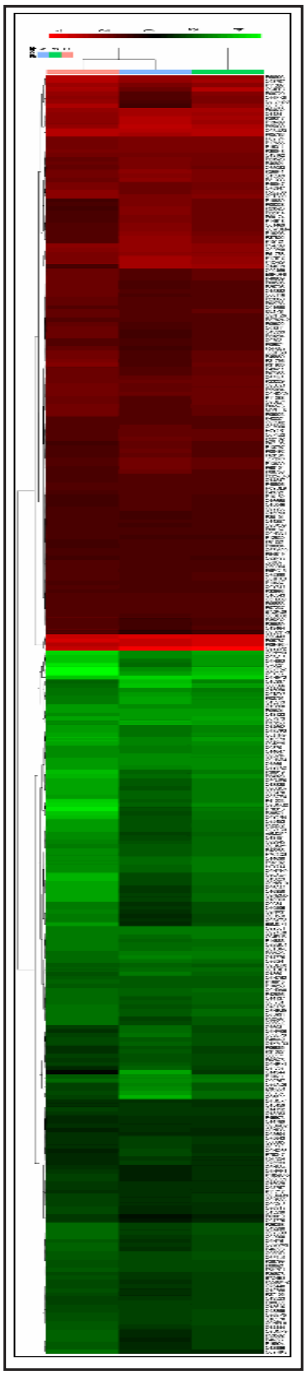

Fig. 4. Heatmap of the expression levels of 312 dysregulated proteins. The red-colored clusters represent up-regulated proteins, and the green-colored clusters represent down-regulated proteins.

Table 2. List of up-regulated proteins in TP-treated A549 cells

Accession NO.	Gene name	Protein name	Fold change (Mean±SD)	P-value (Mean±SD)
O95831-3	AIFM1	Isoform 3 of Apoptosis-inducing factor 1	2.05±0.04	0.15±0.010
P35659	DEK	Protein DEK	2.49±0.45	0.01±0
P35232	PHB	Prohibitin	2.61±0.4	0.01±0.02
Q13464	ROCK1	Rho-associated protein kinase 1	2.75±0.61	0±0
P30101	PDIA3	Protein disulfide-isomerase A3	2.15±0.2	0±0
O43399	TPD54	Tumor protein D54	2.84±0.75	0.05±0
Q9BXJ9	NAA15	N-alpha-acetyltransferase 15, NatA auxiliary subunit	2.1±0.1	0±0
F5H6E2	F5H6E2	Unconventional myosin-Ic	2.67±0.59	0.01±0
P23284	PPIB	Peptidyl-prolyl cis-trans isomerase B	2.94±0.83	0±0
Q15293	RCN1	Reticulocalbin-1	2.14±0.13	0.02±0.01
O60264	SMCA5	SWI/SNF-related matrix-associated actin-dependent regulator of chromatin subfamily A member 5	2.31±0.35	0±0
J9JID7	J9JID7	Lamin B2, isoform CRA_a	2.39±0.36	0±0
Q14257	RCN2	Reticulocalbin-2	2.13±0.06	0±0
Q32P28	P3H1	Prolyl 3-hydroxylase 1	2.05±0.05	0.02±0.02
Q08211	DHX9	ATP-dependent RNA helicase A	2.71±0.7	0±0
P09622	DLDH	Dihydrolipoyl dehydrogenase	2.56±0.34	0.02±0
E9PC15	E9PC15	Acylglycerol kinase	2.28±0.24	0±0
P09874	PARP1	Poly [ADP-ribose] polymerase 1	2.48±0.46	0±0.01
Q5JRX3	PREP	Presequence protease	2.39±0.34	0±0
Q9H3N1	TMX1	Thioredoxin-related transmembrane protein 1	2.19±0.06	0.02±0
P00167	CYB5	Cytochrome b5	2.2±0.07	0.04±0.01
P54819	KAD2	Adenylate kinase 2	2.12±0.07	0.01±0.02
O75390	CISY	Citrate synthase	2.41±0.31	0±0
P21796	VDAC1	Voltage-dependent anion-selective channel protein 1	3.01±0.17	0±0
P30084	ECHM	Enoyl-CoA hydratase	2.11±0.01	0.02±0.01
Q07021	C1QBP	Complement component 1 Q subcomponent-binding protein	2.52±0.47	0.03±0.01
Q6ZMP0	THSD4	Thrombospondin type-1 domain-containing protein 4	2.14±0.07	0.04±0
O00116	ADAS	Alkyldihydroxyacetonephosphate synthase, peroxisomal	2.65±0.6	0.03±0.01
P45880	VDAC2	Voltage-dependent anion-selective channel protein 2	2.93±0.69	0±0
Q9Y617	SERC	Phosphoserine aminotransferase	2.31±0.09	0±0
P61221	ABCE1	ATP-binding cassette sub-family E member 1	2.14±0.15	0±0
J3QRS3	J3QRS3	Myosin regulatory light chain 12A	2.96±1	0.01±0.02
P13667	PDIA4	Protein disulfide-isomerase A4	2.3±0.04	0±0
P25705	ATPA	ATP synthase subunit alpha	2.76±0.36	0±0
P00505	AATM	Aspartate aminotransferase	2.74±0.64	0±0
P33993	MCM7	DNA replication licensing factor MCM7	2.26±0.04	0.03±0.01
Q6DD88	ATLA3	Atlastin-3	2.49±0.27	0±0
Q9Y266	NUDC	Nuclear migration protein nudC	2.21±0.2	0±0
B7ZKQ9	B7ZKQ9	SCARB1 protein	2.53±0.25	0.03±0.01
P07237	PDIA1	Protein disulfide-isomerase	2.54±0.23	0±0
P05556	ITB1	Integrin beta-1	2.46±0.11	0±0
Q15046	SYK	Lysine--tRNA ligase	2.8±0.26	0.01±0.02
O15382	BCAT2	Branched-chain-amino-acid aminotransferase	2.77±0.56	0.02±0.01
Q14847	LASP1	LIM and SH3 domain protein 1	2.35±0.11	0±0
Q5H909	Q5H909	Melanoma-associated antigen D2	2.51±0.13	0.02±0.01
P40939	ECHA	Trifunctional enzyme subunit alpha	2.97±0.71	0±0
Q16543	CDC37	Hsp90 co-chaperone Cdc37	2.52±0.08	0±0
Q16658	FSCN1	Fascin	2.25±0.34	0±0
H0YDL9	H0YDL9	CD81 antigen (Fragment)	2.44±0.06	0.04±0
E9PDF6	E9PDF6	Unconventional myosin-Ib	2.88±0.52	0±0
P05023	AT1A1	Sodium/potassium-transporting ATPase subunit alpha-1	3.17±0.94	0±0
P02786	TFR1	Transferrin receptor protein 1	2.72±0.3	0±0
P48506	GSH1	Glutamate--cysteine ligase catalytic subunit	2.49±0.03	0.01±0.01
P22570-3	ADRO	Isoform 3 of NADPH: adrenodoxin oxidoreductase	2.42±0.16	0±0
Q01650	LAT1	Large neutral amino acids transporter small subunit 1	2.68±0.17	0.01±0.02
O00469	PLOD2	Procollagen-lysine,2-oxoglutarate 5-dioxygenase 2	2.86±0.39	0±0
P16152	CBR1	Carbonyl reductase [NADPH] 1	2.31±0.39	0±0
O95202	LETM1	LETM1 and EF-hand domain-containing protein 1	2.61±0.03	0±0
P23368	MAOM	NAD-dependent malic enzyme	2.78±0.22	0.03±0.01
Q9ULV4	COR1C	Coronin-1C	3.06±0.57	0±0
M0R116	M0R116	Sodium/potassium-transporting ATPase subunit alpha-3	3.13±0.67	0.05±0
P42224	STAT1	Signal transducer and activator of transcription 1-alpha/beta	2.62±0.09	0±0
P49721	PSB2	Proteasome subunit beta type-2	2.41±0.38	0.03±0.02
P11388	TOP2A	DNA topoisomerase 2-alpha	3.07±0.52	0±0
P06576	ATPB	ATP synthase subunit beta	3.13±0.53	0±0
Q9NTZ6	RBM12	RNA-binding protein 12	2.85±0.13	0.01±0.01
P12830	CDH1	Cadherin-1	2.30±0.10	0.04±0.01
P07355	ANXA2	Annexin A2	2.94±0.23	0±0
P27824-2	CALX	Isoform 2 of Calnexin	2.81±0.04	0±0
P49411	EFTU	Elongation factor Tu	3±0.31	0±0
Q96PK6	RBM14	RNA-binding protein 14	3.89±0.53	0.01±0.01
I3L1P8	I3L1P8	Mitochondrial 2-oxoglutarate/malate carrier protein (Fragment)	2.89±0.11	0±0
P55084	ECHB	Trifunctional enzyme subunit beta	3.27±0.51	0.01±0.02
Q6PI48	SYDM	Aspartate--tRNA ligase	3.07±0.22	0±0

continued

Accession NO.	Gene name	Protein name	Fold change (Mean±SD)	P-value (Mean±SD)
Q6PIU2	NCEH1	Neutral cholesterol ester hydrolase 1	2.9±0.13	0±0
Q07960	RHG01	Rho GTPase-activating protein 1	2.72±0.39	0.01±0
P13797	PLST	Plastin-3	2.61±0.66	0±0
P31930	QCR1	Cytochrome b-c1 complex subunit 1	3.18±0.14	0±0
H0Y4R1	H0Y4R1	Inosine-5'-monophosphate dehydrogenase 2 (Fragment)	2.9±0.28	0±0
P07195	LDHB	L-lactate dehydrogenase B chain	2.59±0.77	0±0
O75947	ATP5H	ATP synthase subunit d	3.63±0.71	0.02±0.01
P48047	ATPO	ATP synthase subunit O	3.65±0.73	0.04±0.01
Q9HDC9	APMAP	Adipocyte plasma membrane-associated protein	3.39±0.29	0±0
P23229	ITA6	Integrin alpha-6	3.16±0.08	0±0
P63104	1433Z	14-3-3 protein zeta/delta	2.71±0.77	0±0
O43707	ACTN4	Alpha-actinin-4	6.61±1.84	0±0
Q8IVF2-3	AHNK2	Isoform 3 of Protein AHNAK2	3.94±0.84	0±0
P00492	HPRT	Hypoxanthine-guanine phosphoribosyltransferase	2.75±0.83	0±0
F5GZS6	F5GZS6	4F2 cell-surface antigen heavy chain	4.01±0.91	0±0
P22102	PUR2	Trifunctional purine biosynthetic protein adenosine-3	2.99±0.54	0±0
P08758	ANXA5	Annexin A5	2.85±0.73	0±0
Q13162	PRDX4	Peroxiredoxin-4	3.56±0.05	0.01±0.02
P13639	EF2	Elongation factor 2	2.98±0.38	0±0
J3KR97	J3KR97	Tubulin-specific chaperone D	2.99±0.16	0.01±0.01
P68104	EF1A1	Elongation factor 1-alpha 1	2.98±0.97	0±0
O75083	WDR1	WD repeat-containing protein 1	3.35±0.54	0±0
P08729	K2C7	Keratin, type II cytoskeletal 7	4.32±0.78	0±0
P46821	MAP1B	Microtubule-associated protein 1B	3.5±0.43	0±0
P11387	TOP1	DNA topoisomerase 1	5.03±1.64	0±0
P30048	PRDX3	Thioredoxin-dependent peroxide reductase	3.85±0.03	0.02±0.01
P15311	EZRI	Ezrin	3.79±0.27	0±0
P14618	KPYM	Pyruvate kinase PKM	3.18±1.23	0±0
Q2TB90	HKDC1	Putative hexokinase HKDC1	4.31±0.36	0±0
P23528	COF1	Cofilin-1	3.55±0.71	0±0
Q8IXJ9	ASXL1	Putative Polycomb group protein ASXL1	4.85±1.13	0.04±0.01
P00338	LDHA	L-lactate dehydrogenase A chain	3.09±1.42	0±0
P17655	CAN2	Calpain-2 catalytic subunit	3.81±0.4	0±0
P18669	PGAM1	Phosphoglycerate mutase 1	3.08±1.48	0±0
P60174	TPIS	Triosephosphate isomerase	3.17±1.41	0±0
H0YIV4	H0YIV4	Nucleosome assembly protein 1-like 1 (Fragment)	3.85±0.45	0±0
P22314	UBA1	Ubiquitin-like modifier-activating enzyme 1	3.19±1.5	0±0
P23526	SAHH	Adenosylhomocysteinase	3.15±1.55	0±0
Q8WUM4	PDC6I	Programmed cell death 6-interacting protein	3.43±1.2	0±0
Q01469	FABP5	Fatty acid-binding protein, epidermal	3.41±1.24	0.01±0.01
O15269	SPTC1	Serine palmitoyltransferase 1	4.05±0.5	0.02±0.01
P21333	FLNA	Filamin-A	3.92±1.11	0±0
P18206	VINC	Vinculin	3.62±1.53	0±0
P26641	EF1G	Elongation factor 1-gamma	4.23±0.98	0±0
P61758	PFD3	Prefoldin subunit 3	4.59±0.6	0±0
C9JFR7	C9JFR7	Cytochrome c (Fragment)	5.99±1.32	0±0
P15121	ALDR	Aldose reductase	3.84±1.92	0±0
Q92598	HS105	Heat shock protein 105 kDa	4.88±0.73	0±0
P37802	TAGL2	Transgelin-2	4.12±1.94	0±0
P60903	S10AA	Protein S100-A10	6.33±1.11	0.04±0.01
P54709	AT1B3	Sodium/potassium-transporting ATPase subunit beta-3	5.15±0.7	0.01±0.01
P12429	ANXA3	Annexin A3	5.26±1.65	0±0
P17812	PYRG1	CTP synthase 1	5.27±2.07	0±0
Q14241	ELOA1	Transcription elongation factor B polypeptide 3	6.04±1.33	0.04±0.01
Q14019	COTL1	Coactosin-like protein	5.08±2.79	0±0
P05783	K1C18	Keratin, type I cytoskeletal 18	7.87±1.07	0±0
P04632	CPNS1	Calpain small subunit 1	6.43±0.96	0.03±0.01
P13489	RINI	Ribonuclease inhibitor	6.26±2.27	0.01±0.01
P29317	EPHA2	Ephrin type-A receptor 2	6.39±2.2	0±0
Q9BU23	LMF2	Lipase maturation factor 2	8.28±0.27	0±0
P55039	DRG2	Developmentally regulated GTP-binding protein 2	7.22±2.22	0.04±0
P09493-4	TPM1	Isoform 4 of Tropomyosin alpha-1 chain	10.42±0.2	0.02±0.01
P05787	K2C8	Keratin, type II cytoskeletal 8	11.78±1.3	0±0
O60443	DFNA5	Non-syndromic hearing impairment protein 5	11.92±1.78	0.03±0.01
Q9Y2V2	CHSP1	Calcium-regulated heat stable protein 1	16.91±2.3	0.03±0.02

KEGG pathway analysis

KEGG analysis revealed 30 significant pathways with *P<0.05* (Fig. 3B.). The top ten pathways, including Ribosome biogenesis in eukaryotes (hsa03008), Spliceosome (hsa03040), mRNA surveillance pathway (hsa03015), Carbon metabolism (hsa01200), Steroid biosynthesis (hsa00100), Cysteine and methionine metabolism (hsa00270), Propanoate metabolism (hsa00640), Glycolysis/Gluconeogenesis (hsa00010), Biosynthesis of amino acids (hsa01230), and Cardiac muscle contraction (hsa04260), were displayed. Ribosome biogenesis in eukaryotes and spliceosome were the most significantly enriched pathways (Fig. 6).

Table 3. List of down-regulated proteins in TP-treated A549 cells

Accession NO.	Gene name	Protein name	Fold change (Mean±SD)	P-value (Mean±SD)
Q9H9Y2	RPF1	Ribosome production factor 1	0.06±0.01	0.02±0.01
P02675	FIBB	Fibrinogen beta chain	0.32±0.07	0±0
Q96E29	MTEF3	Transcription termination factor 3	0.21±0.19	0.02±0.01
P37268	FDFT	Squalene synthase	0.11±0.04	0±0
O15213	WDR46	WD repeat-containing protein 46	0.13±0.04	0±0
P02751	FINC	Fibronectin	0.14±0.05	0±0
O00566	MPP10	U3 small nucleolar ribonucleoprotein protein MPP10	0.11±0	0±0
Q8IY37	DHX37	Probable ATP-dependent RNA helicase DHX37	0.21±0.15	0±0
Q13123	RED	Protein Red	0.12±0.01	0±0
Q9Y3C1	NOP16	Nucleolar protein 16	0.07±0.06	0.01±0.01
Q07973	CP24A	1,25-dihydroxyvitamin D(3) 24-hydroxylase	0.1±0.02	0±0
Q15397	K0020	Pumilio domain-containing protein KIAA0020	0.15±0.05	0±0
Q2TAY7	SMU1	WD40 repeat-containing protein SMU1	0.15±0.04	0±0
P09601	HMOX1	Heme oxygenase 1	0.12±0.01	0±0
O00767	ACOD	Acyl-CoA desaturase	0.17±0.06	0±0.01
E9PB61	E9PB61	THO complex subunit 4	0.24±0.16	0±0
Q15050	RRS1	Ribosome biogenesis regulatory protein homolog	0.16±0.04	0±0
Q12860	CNTN1	Contactin-1	0.13±0.01	0±0
Q5VT52	RPRD2	Regulation of nuclear pre-mRNA domain-containing protein 2	0.08±0.07	0.03±0.02
P13611	CSPG2	Versican core protein	0.19±0.07	0.01±0.01
Q9BVJ6	UT14A	U3 small nucleolar RNA-associated protein 14 homolog A	0.11±0.06	0±0
Q9BVI4	NOC4L	Nucleolar complex protein 4 homolog	0.14±0	0±0
O75691	UTP20	Small subunit processome component 20 homolog	0.13±0.02	0±0
Q9H6R4	NOL6	Nucleolar protein 6	0.13±0.03	0±0
Q9NY93	DDX56	Probable ATP-dependent RNA helicase DDX56	0.1±0.07	0±0
O00571	DDX3X	ATP-dependent RNA helicase DDX3X	0.32±0.07	0.02±0.02
Q96AQ6	PBIP1	Pre-B-cell leukemia transcription factor-interacting protein 1	0.24±0.13	0±0
Q9Y3A2	UTP11	Probable U3 small nucleolar RNA-associated protein 11	0.14±0.03	0.04±0.01
C9J2Y9	C9J2Y9	DNA-directed RNA polymerase	0.13±0.04	0±0
Q13573	SNW1	SNW domain-containing protein 1	0.12±0.05	0.03±0.01
O14776	TCRG1	Transcription elongation regulator 1	0.18±0.03	0±0
P22626	ROA2	Heterogeneous nuclear ribonucleoproteins A2/B1	0.18±0.03	0±0
O14647	CHD2	Chromodomain-helicase-DNA-binding protein 2	0.15±0.03	0.04±0.01
Q03701	CEBPZ	CCAAT/enhancer-binding protein zeta	0.15±0.03	0±0
Q9Y4C8	RBM19	Probable RNA-binding protein 19	0.17±0	0.02±0.02
Q5JTH9	RRP12	RRP12-like protein	0.14±0.05	0±0
Q9Y5J1	UTP18	U3 small nucleolar RNA-associated protein 18 homolog	0.17±0.01	0±0
Q13601	KRR1	KRR1 small subunit processome component homolog	0.23±0.07	0±0
Q9NSI2	F207A	Protein FAM207A	0.12±0.08	0.01±0.01
Q9BVP2	GNL3	Guanine nucleotide-binding protein-like 3	0.15±0.05	0.02±0.01
Q53EP0	FND3B	Fibronectin type III domain-containing protein 3B	0.27±0.11	0±0
Q14692	BMS1	Ribosome biogenesis protein BMS1 homolog	0.15±0.06	0±0
Q96I24	FUBP3	Far upstream element-binding protein 3	0.2±0.01	0±0
P24928	RPB1	DNA-directed RNA polymerase II subunit RPB1	0.14±0.08	0±0
P56182	RRP1	Ribosomal RNA processing protein 1 homolog A	0.17±0.04	0±0
Q9NV06	DCA13	DDB1- and CUL4-associated factor 13	0.3±0.15	0±0
O76021	RL1D1	Ribosomal L1 domain-containing protein 1	0.12±0.11	0±0
C9JEU5	C9JEU5	Fibrinogen gamma chain	0.18±0.03	0±0
Q8TDD1	DDX54	ATP-dependent RNA helicase DDX54	0.22±0.02	0±0
Q14690	RRP5	Protein RRP5 homolog	0.17±0.05	0±0
O76031	CLPX	ATP-dependent Clp protease ATP-binding subunit clpX-like	0.29±0.1	0±0
Q9BSC4	NOL10	Nucleolar protein 10	0.2±0.03	0±0
Q8TDN6	BRX1	Ribosome biogenesis protein BRX1 homolog	0.19±0.04	0.01±0.01
Q9ULH0	KDIS	Kinase D-interacting substrate of 220 kDa	0.24±0.03	0±0
Q9NYH9	UTP6	U3 small nucleolar RNA-associated protein 6 homolog	0.17±0.07	0.02±0.02
H0Y714	H0Y714	U3 small nucleolar ribonucleoprotein protein IMP4 (Fragment)	0.18±0.07	0±0
P14866	HNRPL	Heterogeneous nuclear ribonucleoprotein L	0.2±0.04	0±0
Q9UNQ2	DIM1	Probable dimethyladenosine transferase	0.14±0.13	0.04±0
Q1KMD3	HNRL2	Heterogeneous nuclear ribonucleoprotein U-like protein 2	0.28±0.06	0±0
P42696	RBM34	RNA-binding protein 34	0.23±0.01	0.01±0.02
Q9H0A0	NAT10	N-acetyltransferase 10	0.22±0.02	0±0
Q8IV08	PLD3	Phospholipase D3	0.35±0.16	0.01±0.02
Q9BZE4	NOG1	Nucleolar GTP-binding protein 1	0.17±0.09	0±0
P38919	EIF4A3	Eukaryotic initiation factor 4A-III	0.16±0.12	0±0
O95478	NSA2	Ribosome biogenesis protein NSA2 homolog	0.17±0.1	0±0
P48449	ERG7	Lanosterol synthase	0.28±0.04	0±0
P31327	CPSM	Carbamoyl-phosphate synthase [ammonia]	0.33±0.11	0±0
P16615	AT2A2	Sarcoplasmic/endoplasmic reticulum calcium ATPase 2	0.24±0.01	0±0
P10253	LYAG	Lysosomal alpha-glucosidase	0.25±0	0.01±0.01
Q6DKI1	RL7L	60S ribosomal protein L7-like 1	0.22±0.05	0.04±0.01
Q9H7B2	RPF2	Ribosome production factor 2 homolog	0.24±0.01	0.05±0
Q8NEJ9	NGDN	Neuroguidin	0.22±0.05	0±0
Q13838	DX39B	Spliceosome RNA helicase DDX39B	0.17±0.12	0.02±0.02
Q5QJE6	TDIF2	Deoxynucleotidyltransferase terminal-interacting protein 2	0.17±0.12	0.04±0.01
H7C2Q8	H7C2Q8	EBNA1 binding protein 2, isoform CRA_d	0.2±0.08	0±0
P41223	BUD31	Protein BUD31 homolog	0.16±0.14	0.03±0.01
Q9NRX1	PNO1	RNA-binding protein PNO1	0.32±0.08	0±0
P42285	SK2L2	Superkiller viralicidic activity 2-like 2	0.2±0.09	0±0
Q9UMY1	NOL7	Nucleolar protein 7	0.21±0.07	0±0
Q8IY81	SPB1	pre-rRNA processing protein FTSJ3	0.23±0.05	0±0
Q14137	BOP1	Ribosome biogenesis protein BOP1	0.23±0.05	0±0
Q96GQ7	DDX27	Probable ATP-dependent RNA helicase DDX27	0.18±0.13	0±0
P06865	HEXA	Beta-hexosaminidase subunit alpha	0.34±0.09	0±0
P52272	HNRPM	Heterogeneous nuclear ribonucleoprotein M	0.2±0.11	0±0

continued

Accession NO.	Gene name	Protein name	Fold change (Mean±SD)	P-value (Mean±SD)
O43172	PRP4	U4/U6 small nuclear ribonucleoprotein Prp4	0.24±0.07	0±0
Q92945	FUBP2	Far upstream element-binding protein 2	0.22±0.1	0±0
O95453	PARN	Poly(A)-specific ribonuclease PARN	0.2±0.12	0±0
Q6P1J9	CDC73	Parafibromin	0.27±0.03	0±0
Q14344	GNA13	Guanine nucleotide-binding protein subunit alpha-13	0.39±0.12	0.01±0.01
P78316	NOP14	Nucleolar protein 14	0.17±0.18	0±0
Q9Y2R4	DDX52	Probable ATP-dependent RNA helicase DDX52	0.19±0.16	0.01±0.01
P78347	GTF2I	General transcription factor II-I	0.38±0.11	0±0
G3V1C3	G3V1C3	Apoptosis inhibitor 5	0.21±0.13	0±0
Q9NW13	RBM28	RNA-binding protein 28	0.2±0.15	0±0
Q86SJ2	AMGO2	Amphoterin-induced protein 2	0.25±0.08	0±0
Q13823	NOG2	Nucleolar GTP-binding protein 2	0.2±0.16	0±0
Q13151	ROA0	Heterogeneous nuclear ribonucleoprotein A0	0.22±0.13	0.04±0.01
Q96RT1	LAP2	Protein LAP2	0.28±0.04	0.01±0.01
P08621	RU17	U1 small nuclear ribonucleoprotein 70 kDa	0.3±0.03	0±0
Q9NQ55	SSF1	Suppressor of SWI4 1 homolog	0.4±0.12	0.01±0.01
F5H7P7	F5H7P7	Peptidylprolyl isomerase domain and WD repeat-containing protein 1	0.29±0.04	0.02±0.01
P28799	GRN	Granulins	0.3±0.03	0.03±0.01
Q96AE4	FUBP1	Far upstream element-binding protein 1	0.21±0.17	0±0
P38571	LICH	Lysosomal acid lipase/cholesteryl ester hydrolase	0.19±0.18	0.02±0.02
A8MXP9	A8MXP9	Matrin-3	0.23±0.14	0±0
O60885	BRD4	Bromodomain-containing protein 4	0.38±0.07	0±0
P52597	HNRPF	Heterogeneous nuclear ribonucleoprotein F	0.26±0.1	0±0
O43395	PRPF3	U4/U6 small nuclear ribonucleoprotein Prp3	0.32±0.03	0±0
Q9Y3B9	RRP15	RRP15-like protein	0.28±0.09	0.02±0.01
O75643	U520	U5 small nuclear ribonucleoprotein 200 kDa helicase	0.38±0.05	0±0
Q13263	TIF1B	Transcription intermediary factor 1-beta	0.22±0.17	0±0
Q8IX12	CCAR1	Cell division cycle and apoptosis regulator protein 1	0.4±0.08	0±0
Q9NZM5	GSCR2	Glioma tumor suppressor candidate region gene 2 protein	0.22±0.18	0.02±0.01
O43290	SNUT1	U4/U6.U5 tri-snRNP-associated protein 1	0.28±0.11	0.01±0.01
Q13616	CUL1	Cullin-1	0.33±0.04	0.01±0
F8VUJ3	F8VUJ3	Polypeptide N-acetylgalactosaminyltransferase	0.35±0.01	0.01±0.02
Q9NPL8	TIDC1	Complex I assembly factor TIMMDC1	0.3±0.07	0.01±0.01
Q10570	CPSF1	Cleavage and polyadenylation specificity factor subunit 1	0.32±0.06	0±0
Q96EP5	DAZP1	DAZ-associated protein 1	0.32±0.06	0±0
O75533	SF3B1	Splicing factor 3B subunit 1	0.42±0.08	0±0.01
P26368	U2AF2	Splicing factor U2AF 65 kDa subunit	0.28±0.12	0.01±0.01
Q13523	PRP4B	Serine/threonine-protein kinase PRP4 homolog	0.35±0.03	0.03±0.01
F5H324	F5H324	Arylsulfatase E	0.43±0.07	0±0
Q13283	G3BP1	Ras GTPase-activating protein-binding protein 1	0.38±0	0.01±0.01
Q16850	CP51A	Lanosterol 14-alpha demethylase	0.24±0.19	0.03±0.01
B7Z4B8	B7Z4B8	Heterogeneous nuclear ribonucleoprotein U-like protein 1	0.33±0.07	0±0
Q15459	SF3A1	Splicing factor 3A subunit 1	0.41±0.03	0±0
Q96A72	MGN2	Protein mago nashi homolog 2	0.24±0.2	0.01±0.01
Q14152	EIF3A	Eukaryotic translation initiation factor 3 subunit A	0.38±0.01	0±0
P36578	RL4	60S ribosomal protein L4	0.34±0.07	0±0
O60506	HNRPQ	Heterogeneous nuclear ribonucleoprotein Q	0.28±0.16	0±0
Q8WVV9	HNRLL	Heterogeneous nuclear ribonucleoprotein L-like	0.31±0.11	0.03±0.02
Q14444	CAPR1	Caprin-1	0.33±0.1	0.01±0.02
Q92900	RENT1	Regulator of nonsense transcripts 1	0.3±0.14	0.05±0
O75448	MED24	Mediator of RNA polymerase II transcription subunit 24	0.36±0.06	0.03±0.01
Q00341	VIGLN	Vigilin	0.28±0.17	0±0
Q14789	GOGB1	Golgin subfamily B member 1	0.44±0.04	0±0
P55884-2	EIF3B	Isoform 2 of Eukaryotic translation initiation factor 3 subunit B	0.36±0.06	0.04±0.01
Q9UNX4	WDR3	WD repeat-containing protein 3	0.41±0	0.01±0.02
Q9NY61	AATF	Protein AATF	0.32±0.12	0.01±0
Q9H583	HEAT1	HEAT repeat-containing protein 1	0.38±0.05	0.01±0
P45973	CBX5	Chromobox protein homolog 5	0.44±0.03	0.01±0
Q9NV31	IMP3	U3 small nucleolar ribonucleoprotein protein IMP3	0.28±0.19	0.03±0
P46776	RL27A	60S ribosomal protein L27a	0.32±0.14	0.04±0
Q92797	SYMPK	Symplekin	0.41±0.03	0±0
Q8NI36	WDR36	WD repeat-containing protein 36	0.46±0.04	0±0
Q9UKM9	RALY	RNA-binding protein Raly	0.38±0.07	0±0
P27105	STOM	Erythrocyte band 7 integral membrane protein	0.36±0.1	0±0
Q9UKD2	MRT4	mRNA turnover protein 4 homolog	0.44±0.01	0±0
Q6YHK3	CD109	CD109 antigen	0.36±0.11	0.01±0
Q12788	TBL3	Transducin beta-like protein 3	0.36±0.12	0.01±0
Q15029	U5S1	116 kDa U5 small nuclear ribonucleoprotein component	0.42±0.04	0±0
Q9C0J8	WDR33	pre-mRNA 3' end processing protein WDR33	0.4±0.07	0.03±0
P11717	MPRI	Cation-independent mannose-6-phosphate receptor	0.43±0.03	0.01±0
Q9BYG3	MK67I	MKI67 FHA domain-interacting nucleolar phosphoprotein	0.31±0.2	0.01±0
Q12996	CSTF3	Cleavage stimulation factor subunit 3	0.35±0.15	0.01±0
B5MCF9	B5MCF9	Pescadillo homolog	0.28±0.25	0±0
Q9H501	ESF1	ESF1 homolog	0.31±0.21	0.01±0
Q92604	LGAT1	Acyl-CoA:lysophosphatidylglycerol acyltransferase 1	0.46±0.01	0.03±0
P15924	DESP	Desmoplakin	0.36±0.16	0.01±0
P53582	MAP11	Methionine aminopeptidase 1	0.35±0.18	0.01±0
O15230	LAMA5	Laminin subunit alpha-5	0.4±0.11	0.03±0
Q9UNP9	PPIE	Peptidyl-prolyl cis-trans isomerase E	0.35±0.18	0±0
Q96ST2	IWS1	Protein IWS1 homolog	0.4±0.11	0.02±0
Q9NVP1	DDX18	ATP-dependent RNA helicase DDX18	0.44±0.02	0.05±0
Q9BQ39	DDX50	ATP-dependent RNA helicase DDX50	0.40±0.08	0.03±0
P46777	RL5	60S ribosomal protein L5	0.36±0.10	0.01±0
Q8N684	CPSF7	Cleavage and polyadenylation specificity factor subunit 7	0.45±0.05	0.03±0
P18583-5	SON	Isoform D of Protein SON	0.40±0.09	0.05±0
O94776	MTA2	Metastasis-associated protein MTA2	0.38±0.12	0±0
P63010	AP2B1	AP-2 complex subunit beta	0.34±0.15	0.01±0

Protein-protein interaction network analysis

To further examine the comprehensive information obtained from the identified protein data, the PPI network was analyzed. The network model was generated using the Cytoscape web application based on information gained in up to 4 levels of functional analysis: fold-change of gene/protein expression, protein-protein interactions, KEGG pathway enrichment and biological process enrichment. A merged network is shown in Fig. 7. Again, PPI analysis identified ribosome biogenesis in eukaryotes and the spliceosome as the most significantly enriched pathways. In the network, the proteins indicated with red circle nodes were up-regulated, and the proteins indicated with green circle nodes were down-regulated. These data clearly show that most of the proteins were down-regulated in Ribosome biogenesis in eukaryotes, Spliceosome, and mRNA surveillance pathways, while the dysregulated proteins in Cysteine and methionine metabolism, Propanoate metabolism and Glycolysis/Gluconeogenesis were up-regulated.

Table 4: The 50 apoptosis-associated proteins of enrichment analysis

Accession NO.	Gene name	Protein name	Fold change (Mean±SD)	P-value (Mean±SD)
P35232	PHB	Prohibitin	2.61±0.4	0.01±0.02
Q13464	ROCK1	Rho-associated protein kinase 1	2.75±0.61	0±0
P30101	PDIA3	Protein disulfide-isomerase A3	2.15±0.2	0±0
Q9BXJ9	NAA15	N-alpha-acetyltransferase 15, NatA auxiliary subunit	2.1±0.1	0±0
P09874	PARP1	Poly [ADP-ribose] polymerase 1	2.48±0.46	0±0.01
P21796	VDAC1	Voltage-dependent anion-selective channel protein 1	3.01±0.17	0±0
Q07021	C1QBP	Complement component 1 Q subcomponent-binding protein	2.52±0.47	0.03±0.01
P45880	VDAC2	Voltage-dependent anion-selective channel protein 2	2.93±0.69	0±0
P07237	PDIA1	Protein disulfide-isomerase	2.54±0.23	0±0
P05556	ITB1	Integrin beta-1	2.46±0.11	0±0
P48506	GSH1	Glutamate--cysteine ligase catalytic subunit	2.49±0.03	0.01±0.01
P42224	STAT1	Signal transducer and activator of transcription 1-alpha/beta	2.62±0.09	0±0
P49721	PSB2	Proteasome subunit beta type-2	2.41±0.38	0.03±0.02
P11388	TOP2A	DNA topoisomerase 2-alpha	3.07±0.52	0±0
P12830	CDH1	Cadherin-1	2.30±0.10	0.04±0.01
P23229	ITA6	Integrin alpha-6	3.16±0.08	0±0
P63104	1433Z	14-3-3 protein zeta/delta	2.71±0.77	0±0
O43707	ACTN4	Alpha-actinin-4	6.61±1.84	0±0
P08758	ANXA5	Annexin A5	2.85±0.73	0±0
P08729	K2C7	Keratin, type II cytoskeletal 7	4.32±0.78	0±0
P11387	TOP1	DNA topoisomerase 1	5.03±1.64	0±0
P30048	PRDX3	Thioredoxin-dependent peroxide reductase	3.85±0.03	0.02±0.01
P14618	KPYM	Pyruvate kinase PKM	3.18±1.23	0±0
P23528	COF1	Cofilin-1	3.55±0.71	0±0
P00338	LDHA	L-lactate dehydrogenase A chain	3.09±1.42	0±0
Q8WUM4	PDC6I	Programmed cell death 6-interacting protein	3.43±1.2	0±0
P21333	FLNA	Filamin-A	3.92±1.11	0±0
P15121	ALDR	Aldose reductase	3.84±1.92	0±0
Q92598	HS105	Heat shock protein 105 kDa	4.88±0.73	0±0
P05783	K1C18	Keratin, type I cytoskeletal 18	7.87±1.07	0±0
P04632	CPNS1	Calpain small subunit 1	6.43±0.96	0.03±0.01
P29317	EPHA2	Ephrin type-A receptor 2	6.39±2.2	0±0
P05787	K2C8	Keratin, type II cytoskeletal 8	11.78±1.3	0±0
O60443	DFNA5	Non-syndromic hearing impairment protein 5	11.92±1.78	0.03±0.01
P02675	FIBB	Fibrinogen beta chain	0.32±0.07	0±0
P09601	HMOX1	Heme oxygenase 1	0.12±0.01	0±0
O00571	DDX3X	ATP-dependent RNA helicase DDX3X	0.32±0.07	0.02±0.02
Q9Y3A2	UTP11	Probable U3 small nucleolar RNA-associated protein 11	0.14±0.03	0.04±0.01
Q13573	SNW1	SNW domain-containing protein 1	0.12±0.05	0.03±0.01
O76021	RL1D1	Ribosomal L1 domain-containing protein 1	0.12±0.11	0±0
Q6P1J9	CDC73	Parafibromin	0.27±0.03	0±0
Q14344	GNA13	Guanine nucleotide-binding protein subunit alpha-13	0.39±0.12	0.01±0.01
Q86SJ2	AMGO2	Amphoterin-induced protein 2	0.25±0.08	0±0
Q8IX12	CCAR1	Cell division cycle and apoptosis regulator protein 1	0.4±0.08	0±0
Q9NZM5	GSCR2	Glioma tumor suppressor candidate region gene 2 protein	0.22±0.18	0.02±0.01
O43290	SNUT1	U4/U6.U5 tri-snRNP-associated protein 1	0.28±0.11	0.01±0.01
Q13616	CUL1	Cullin-1	0.33±0.04	0.01±0
Q9NY61	AATF	Protein AATF	0.32±0.12	0.01±0
P11717	MPRI	Cation-independent mannose-6-phosphate receptor	0.43±0.03	0.01±0
P15924	DESP	Desmoplakin	0.36±0.16	0.01±0

Evaluation of iTRAQ results using western blotting

Based on the results of the MS analysis, the expression levels of five dysregulated proteins were validated using western blotting in TP-treated or negative control cells. The expression levels of two proteins (MTA2 and EIF4A3) were significantly down-regulated (Fig. 8A), while the expression levels of the remaining three proteins (PHB, CDH1 and AIFM1) were markedly increased in TP-treated cells compared with the corresponding control (Fig. 8B), consistent with the results from the MS analysis. Therefore, the altered expression levels of 312 proteins were considered induced by TP.

Discussion

TP has been widely investigated for its broad-spectrum anticancer activity. Many studies have shown that TP inhibits cell growth and induces apoptosis in various cancers,

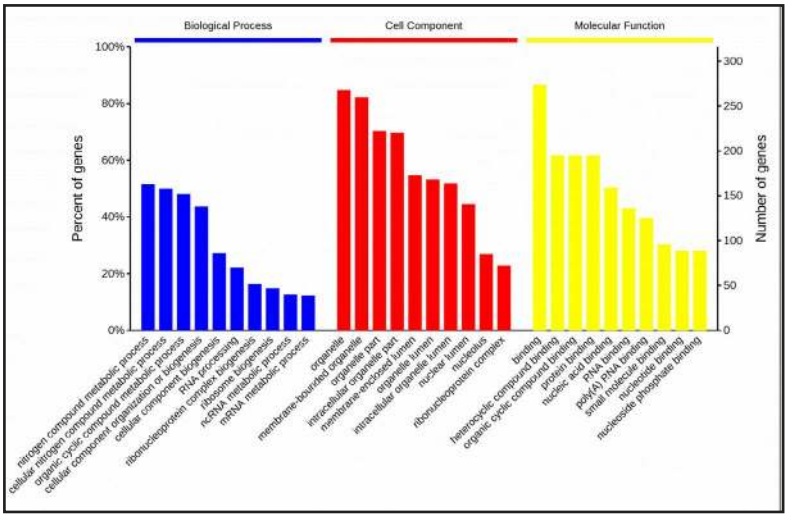

Fig. 5. GO enrichment analysis. An overview of the GO annotations of the 312 dysregulated proteins with up to 10 significantly enriched terms in three categories: biological process (BP), cellular component (CC) and molecular function (MF). The cutoff of P-value was set to 0.05. Terms in the same category were ordered based on the P-values. Information for the percentages and numbers of involved genes/proteins in a term is provided on the left and right y-axes.

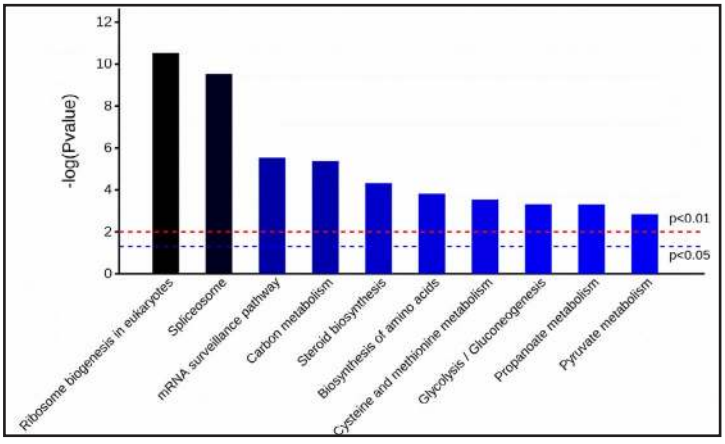

Fig. 6. Distribution of enriched KEGG pathways. Columns refer to related pathways, colored with gradient colors from midnight blue (smaller P-value) to lighter blue (larger P-value).

primarily through multiple mechanisms, including the suppression of various signaling pathways and proliferative and antiapoptotic factors in a given cell type and under specific conditions. TP has been reported to strongly inhibit the transcription of numerous pro-inflammatory mediators [25]and was also implicated as a potent inhibitor of NF-kappa B and a promoter of transcriptional arrest [26-30]. Recent studies have shown that TP inhibits RNA polymerase-mediated transcription by targeting transcription factors, leading to the down-regulation of certain mRNA molecules [31-33]. However, to our knowledge, there are no studies reporting the anti-proliferative and pro-apoptotic effects of TP against NSCLC cells at the proteomics level. In the present study, we attempted to investigate the potential protein targets of TP in a human NSCLC A549 lung adenocarcinoma cell line *in vitro*. First, we investigated the cytotoxicity of TP on A549 cells. TP strongly inhibited cell proliferation and induced cell apoptosis and cell cycle arrest in dose-dependent manners. Second, an iTRAQ-based proteomics method was employed to analyze the molecular targets of A549 cancer cells after TP treatment, and pathway and network analyses were performed. Proteomics analysis is a powerful tool for the identification of biological markers and estimation of biological networks [34]. A global view of the inter-connectivity of signaling proteins and their actions is critically important for successful lung cancer therapy [35] and should provide a comprehensive perspective for elucidating the roles of TP as a potential agent for treatment of NSCLC. We observed 312 differentially expressed proteins in A549 cells after TP treatment. Moreover, bioinformatics analysis revealed that these proteins were involved in many BPs, including ribosome biogenesis, RNA processing, ribonucleoprotein

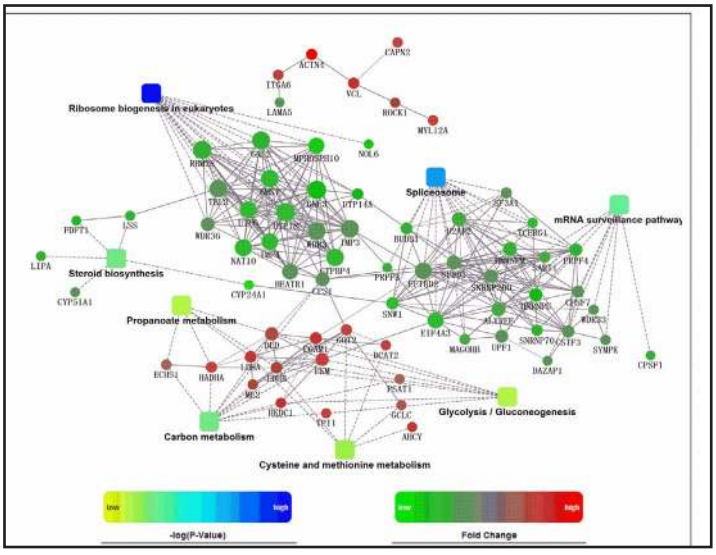

Fig. 7. Protein-protein interaction (PPI) network. The PPI analysis was based on fold changes of protein expression, PPIs, and KEGG pathway and biological process enrichments. Circle nodes refer to genes/proteins. The rectangles refer to KEGG pathways or biological processes, colored with gradient colors from yellow (smaller P-value) to blue (larger P-value). Genes/proteins are colored in red (up-regulation) and green (down-regulation). A default confidence cutoff of 400 was used: interactions with higher confidence scores are shown as solid lines between genes/proteins or are otherwise indicated as dashed lines.

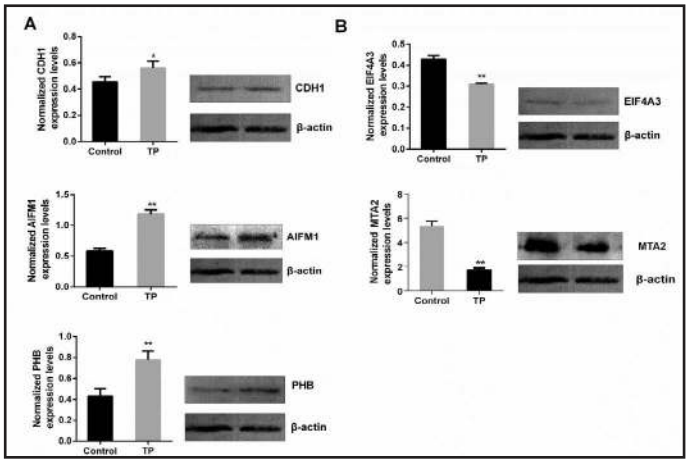

Fig. 8. Expression levels of the representative dysregulated proteins were verified using western blot analysis. (A) CDH1, AIFM1 and PHB are down-regulated proteins. (B) EIF4A3 and MTA2 are up-regulated proteins. β-actin was used as the loading control. Data are expressed as the means ± SD (n=3). *P<0.05 and **P<0.01 compared with the control group.

complex biogenesis, rRNA metabolic process, rRNA processing, ncRNA processing, cellular component biogenesis, and others. These proteins were implicated in 226 different KEGG pathways and associated with each other to form a network. The anticancer activity of TP against A549 cancer cells is mediated through its effects on multiple BPs and pathways, including ribosome biogenesis in eukaryotes, the spliceosome, mRNA surveillance pathway, PARP1/AIF pathway, metabolic pathway and other important molecular targets.

Ribosome biogenesis in eukaryotes and spliceosome and mRNA surveillance pathways are central processes for gene expression and protein synthesis, which are inextricably associated with cell growth and division. After TP treatment, most of the differentially expressed proteins involved in RNA metabolism pathways were significantly down-regulated. Among these down-regulated proteins, SNW1, HNRPM, EFTUD2, and SNRNP200 are components of the spliceosome. Many drugs have recently been demonstrated as inhibitors of RNA splicing, with cytotoxic effects on tumor cell lines [36]. SNW1 depletion induced apoptosis in breast cancer cells, and EFTUD2 knockdown also significantly promoted cellular apoptosis [37]. Previous studies have demonstrated that through the inhibition of the Akt signaling pathway, TP induces Bax- and Bcl-2-mediated mitochondrial apoptotic pathways, resulting in caspase-9- and caspase-3-triggered cell apoptosis [17, 38, 39]. In the present study, we identified key nuclear proteins and other mitochondrial proteins as down- or upstream targets of the Akt signaling pathway, such as REF1/Aly, GTPBP4, EIF4A3 and PHB.

REF1/Aly, GTPBP4 and EIF4A3 are involved in RNA metabolism-related pathways. EIF4A3 (DDX48) is a core component of the exon junction complex (EJC) and plays a critical role in multiple posttranscriptional events, including RNA subcellular localization, nonsense-mediated decay (NMD), and translation [40]. The AKT signaling pathway regulates the assembly of the core EJC proteins eIF4A3, MAGOH, and Y14 into complexes at speckled domains, which is essential for mRNA export. AKT inhibition results in the disorder of mRNA export and gene expression [41]. REF1/Aly is a nuclear speckle protein implicated in mRNA export and is a physiological target of the nuclear Akt signaling cascade [42, 43]. The depletion of Aly markedly blocks cell cycle progression and reduces cell growth and mRNA export, and these processes are regulated by Akt phosphorylation [43, 44]. GTPBP4, located in the nucleus, is involved in the biosynthesis of the 60S subunit of the ribosome [45] and can be used as a molecular switch to control signal transduction pathways, protein synthesis and other biological processes. GTPBP4 down-regulation in colorectal cancer cell lines significantly inhibited cell proliferation [46]. GTPBP4 is closely associated with the MAPK signaling pathway and participates in the regulation of MAPK and Akt signaling pathways through interactions with AKT [47, 48]. It has also been reported that GTPBP4 binds to P53, and low GTPBP4 expression leads to the aggregation and activation of P53 proteins, which regulate the downstream apoptosis-related factors caspase-3, caspase-9, and PARP [49]. Prohibitin belongs to the Band-7 protein family and is widely present in different cellular compartments. Several studies using different organism models have provided strong evidence for critical biological roles of PHB in mitochondrial function, cell proliferation, and development. The contribution of PHB to cancer cell apoptosis may depend on the stimuli and cell type [50]. Recent studies have characterized PHB as a multifunctional protein involved in the PI3K/Akt and Ras/MAPK/ERK signaling pathways. A recent study in cancer cells showed that Akt phosphorylates PHB at Thr258. PHB could also indirectly facilitate crosstalk between the PI3K/Akt and Ras/MAPK/ERK pathways through interactions with their signaling intermediates. The emerging roles of PHB in the PI3K/Akt and Ras/ERK pathways highlight the importance of PHB in the crosstalk between signaling pathways. In the present study, PHB was up-regulated in the TP-induced apoptosis of NSCLC cells. We speculate that PHB may play an important role in the TP-induced apoptosis of A549 cells. Targeting PHB may have inspiring prospects in the future research of TP anti-tumor activity.

As described above, we speculated that TP-induced toxicities in lung cancer cells may be associated with the inhibition of RNA metabolism-related pathways, regulated by the Akt signaling pathway via important molecular target proteins. TP inhibits global ribosome biogenesis and splicing in cancer cells, which may explain the high potency of TP in killing lung cancer. Further studies are required to determine the potential link between the target proteins induced by TP and lung cancer and to provide a new strategy for cancer therapy.

Apoptosis-inducing factor 1 (AIFM1) is a mitochondrial flavoprotein with a critical role in programmed cell death. AIFM1 is a cell death executioner alternative to caspases [51]. Distinguishing from classic caspase-dependent apoptosis, the PARP1/AIF death cascade is a highly orchestrated and caspase-independent programmed cell death process termed parthanatos [52, 53]. In the present study, both AIF and PARP1 were up-regulated in NSCLC A549 cells after TP treatment, indicating that in addition to the classic caspase-dependent apoptosis pathway [17], the PARP1/AIF pathway may be another mechanism for TP to induce lung cancer cell apoptosis.

Unlike normal human cells, cancer cells display metabolic reprogramming to meet cell growth and proliferation needs [54]. Altered metabolic pathways in cancer cells may be attractive targets for anticancer therapy [55]. In the present study, some proteins related to metabolic pathways were dysregulated after TP treatment. The dysregulated proteins ECHS1, HADHA, PKM, AHCY and GOT2 are located in the mitochondria, and these enzymes are involved in apoptosis initiation and development. The mitochondrion is an important organelle with multiple functions, including ATP production, lipid metabolism, developmental processes and apoptosis regulation [56]. The expression levels of these proteins were enhanced during TP-induced apoptosis, suggesting that apoptosis is an active

and energy-consuming procedure. These results demonstrated that energy metabolism is important in TP-induced apoptosis. Further research is required to determine the potential link between the altered mitochondrial enzymes induced by TP and NSCLC and to provide a new strategy for NSCLC therapy.

Metastasis is the ultimate cause of death for most cancer patients. TP has been reported as an inhibitor of lung cancer cell migration and metastasis, but its mechanism is not clearly defined [12, 57, 58]. We observed some other differentially expressed proteins, such as MTA2 and E-cadherin (CDH1), implicated in cancer cell migration. MTA2 is a member of the metastasis tumor-associated family of transcriptional regulators and acts as a central regulator of key gene expression pathways central to metastatic dissemination [59]. MTA2 knockdown in human cancer cells significantly inhibited migration and invasion [60]. E-cadherin is the core protein of the epithelial adherens junction. The loss of E-cadherin expression is a crucial step in the epithelial-mesenchymal transition (EMT) and is involved in cancer invasion and metastasis [61]. In human tumors, E-cadherin down-regulation is frequently associated with poor prognosis [62, 63]. Interestingly, MTA2 promotes NSCLC metastasis through E-cadherin inhibition [64]. In the present study, we observed that TP not only up-regulates E-cadherin but also down-regulates MTA2, which might be a new target of the TP-mediated inhibition of A549 cell migration.

In conclusion, TP showed significant cytotoxicity in human A549 lung cancer cells, induced cell apoptosis and blocked cell cycle arrest. Potential cytotoxicity mechanisms were explored using an iTRAQ-based proteomics approach. The results provided the first evidence that the broad-spectrum anti-tumor activity of TP in lung cancer cells may be associated with inhibition of RNA metabolism and protein synthesis. Among the large number of differentially expressed proteins identified, some proteins, which may be potential targets for lung cancer treatment in the future, were validated. The present study provides an effective platform for the anticancer activity of TP. However, the present study has several limitations. First, there is a lack of the same experiments on normal lung cells. Second, protein profile changes in normal lung cells in response to TP may better reveal the specificity of TP effects on cancer cells. Moreover, the *in vivo* activity, clinical application, and other mechanisms of TP against NSCLC require further investigation.

Abbreviations

TP (triptolide); PNCA-1 (pancreatic cancer cells); NSCLC (non-small cell lung cancer); iTRAQ (isobaric tags for relative and absolute quantitation); NanoLC-MS/MS (nano liquid chromatography-mass spectrometry); FBS (fetal bovine serum); DMSO (dimethylsulfoxide); BCA (bicinchoninic acid); PI (propidium iodide); PMSF (phenylmethanesulfonyl fluoride); BP (biological process); CC (cellular component); KEGG (Kyoto Encyclopedia of Genes and Genomes); MF (molecular function); SDS-PAGE (sodium dodecyl sulfate-polyacrylamide gel electrophoresis); PVDF (polyvinylidene fluoride); GO (Gene Ontology); HP-RP (high-pH reverse phase); CE (collision energy); FDR (false discovery rate.);

Acknowledgements

This study was financially supported by grants from the Science Foundation from the Science and Technology Project of Zhejiang Province (2014F10014) and the Natural Science Foundation of Zhejiang Province (Q17H290005). This study was also supported by National Science Foundation of China (No. 81774026).

Disclosure Statement

No conflicts of interest exist in the submission of this manuscript, and this manuscript was approved by all authors for publication.

References

1 Torre LA, Siegel RL, Jemal A: Lung Cancer Statistics. Adv Exp Med Biol 2016;893:1-19.
2 Mizuno K, Mataki H, Seki N, Kumamoto T, Kamikawaji K, Inoue H: MicroRNAs in non-small cell lung cancer and idiopathic pulmonary fibrosis. J Hum Genet 2016.
3 Deng W, Yan M, Yu T, Ge H, Lin H, Li J, Liu Y, Geng Q, Zhu M, Liu L, He X, Yao M: Quantitative proteomic analysis of the metastasis-inhibitory mechanism of miR-193a-3p in non-small cell lung cancer. Cell Physiol Biochem 2015;35:1677-1688.
4 Rajeswaran A, Trojan A, Burnand B, Giannelli M: Efficacy and side effects of cisplatin- and carboplatin-based doublet chemotherapeutic regimens versus non-platinum-based doublet chemotherapeutic regimens as first line treatment of metastatic non-small cell lung carcinoma: a systematic review of randomized controlled trials. Lung Cancer 2008;59:1-11.
5 Kupchan SM, Court WA, Dailey RG, Jr., Gilmore CJ, Bryan RF: Triptolide and tripdiolide, novel antileukemic diterpenoid triepoxides from Tripterygium wilfordii. J Am Chem Soc 1972;94:7194-7195.
6 Corson TW, Crews CM: Molecular understanding and modern application of traditional medicines: triumphs and trials. Cell 2007;130:769-774.
7 Sun S, Wang Y, Zhou Y: [Research progress on immunosuppressive activity of monomers extracted from Chinese medicine]. Zhongguo Zhong Yao Za Zhi 2010;35:393-396.
8 Ziaei S, Halaby R: Immunosuppressive, anti-inflammatory and anti-cancer properties of triptolide: A mini review. Avicenna J Phytomed 2016;6:149-164.
9 Li J, Liu R, Yang Y, Huang Y, Li X, Liu R, Shen X: Triptolide-induced *in vitro* and *in vivo* cytotoxicity in human breast cancer stem cells and primary breast cancer cells. Oncol Rep 2014;31:2181-2186.
10 Mujumdar N, Banerjee S, Chen Z, Sangwan V, Chugh R, Dudeja V, Yamamoto M, Vickers SM, Saluja AK: Triptolide activates unfolded protein response leading to chronic ER stress in pancreatic cancer cells. Am J Physiol Gastrointest Liver Physiol 2014;306:G1011-1020.
11 Wang Y, Liu T, Li H: Enhancement of triptolide-loaded micelles on tumorigenicity inhibition of human ovarian cancer. J Biomater Sci Polym Ed 2016;27:545-556.
12 Reno TA, Kim JY, Raz DJ: Triptolide Inhibits Lung Cancer Cell Migration, Invasion, and Metastasis. Ann Thorac Surg 2015;100:1817-1824; discussion 1824-1815.
13 Zhao F, Huang W, Zhang Z, Mao L, Han Y, Yan J, Lei M: Triptolide induces protective autophagy through activation of the CaMKKbeta-AMPK signaling pathway in prostate cancer cells. Oncotarget 2016;7:5366-5382.
14 Nakazato T, Sagawa M, Kizaki M: Triptolide induces apoptotic cell death of multiple myeloma cells via transcriptional repression of Mcl-1. Int J Oncol 2014;44:1131-1138.
15 Cheng X, Shi W, Zhao C, Zhang D, Liang P, Wang G, Lu L: Triptolide sensitizes human breast cancer cells to tumor necrosis factoralphainduced apoptosis by inhibiting activation of the nuclear factorkappaB pathway. Mol Med Rep 2016;13:3257-3264.
16 Li Y, Hu S: Triptolide sensitizes liver cancer cell lines to chemotherapy *in vitro* and *in vivo*. Panminerva Med 2014;56:211-220.
17 Meng G, Wang W, Chai K, Yang S, Li F, Jiang K: Combination treatment with triptolide and hydroxycamptothecin synergistically enhances apoptosis in A549 lung adenocarcinoma cells through PP2A-regulated ERK, p38 MAPKs and Akt signaling pathways. Int J Oncol 2015;46:1007-1017.
18 Seo J, Lee KJ: Post-translational modifications and their biological functions: proteomic analysis and systematic approaches. J Biochem Mol Biol 2004;37:35-44.
19 Blackstock WP, Weir MP: Proteomics: quantitative and physical mapping of cellular proteins. Trends Biotechnol 1999;17:121-127.
20 Usami M, Mitsunaga K: Proteomic analysis and *in vitro* developmental toxicity tests for mechanism-based safety evaluation of chemicals. Expert Rev Proteomics 2011;8:153-155.
21 Huang Q, Zhang J, Peng S, Du M, Ow S, Pu H, Pan C, Shen H: Proteomic analysis of perfluorooctane sulfonate-induced apoptosis in human hepatic cells using the iTRAQ technique. J Appl Toxicol 2014;34:1342-1351.
22 Chen H, Xu L, Yin L, Xu Y, Han X, Qi Y, Zhao Y, Liu K, Peng J: iTRAQ-based proteomic analysis of dioscin on human HCT-116 colon cancer cells. Proteomics 2014;14:51-73.
23 Zieske LR: A perspective on the use of iTRAQ reagent technology for protein complex and profiling studies. J Exp Bot 2006;57:1501-1508.

24 Ma S, Sun Y, Zhao X, Xu P: [Recent advance in high accuracy iTRAQ for quantitative proteomics]. Sheng Wu Gong Cheng Xue Bao 2014;30:1073-1082.
25 Wu Y, Cui J, Bao X, Chan S, Young DO, Liu D, Shen P: Triptolide attenuates oxidative stress, NF-kappaB activation and multiple cytokine gene expression in murine peritoneal macrophage. Int J Mol Med 2006;17:141-150.
26 Leuenroth SJ, Crews CM: Triptolide-induced transcriptional arrest is associated with changes in nuclear substructure. Cancer Research 2008;68:5257-5266.
27 Oliveira AR, Beyer G, Chugh R, Skube SJ, Majumder K, Banerjee S, Sangwan V, Li L, Dawra RK, Subramanian S, Saluja AK, Dudeja V: Triptolide abrogates growth of colon cancer and induces cell cycle arrest by inhibiting transcriptional activation of E2F. Lab Invest 2015;95:648-659.
28 Park SW, Kim YI: Triptolide induces apoptosis of PMA-treated THP-1 cells through activation of caspases, inhibition of NF-kappaB and activation of MAPKs. Int J Oncol 2013;43:1169-1175.
29 Ou CC, Chen YW, Hsu SC, Sytwu HK, Loh SH, Li JW, Liu JY: Triptolide Transcriptionally Represses HER2 in Ovarian Cancer Cells by Targeting NF-kappaB. Evid Based Complement Alternat Med 2012;2012:350239.
30 Chen M, Shi JT, Lv ZQ, Huang LJ, Lin XL, Zhang W, Liang RY, Li YQ, Jiang SP: Triptolide inhibits TGF-beta1 induced proliferation and migration of rat airway smooth muscle cells by suppressing NF-kappaB but not ERK1/2. Immunology 2014.
31 Huang M, Zhang H, Liu T, Tian D, Gu L, Zhou M: Triptolide inhibits MDM2 and induces apoptosis in acute lymphoblastic leukemia cells through a p53-independent pathway. Mol Cancer Ther 2013;12:184-194.
32 Titov DV, Gilman B, He QL, Bhat S, Low WK, Dang Y, Smeaton M, Demain AL, Miller PS, Kugel JF, Goodrich JA, Liu JO: XPB, a subunit of TFIIH, is a target of the natural product triptolide. Nat Chem Biol 2011;7:182-188.
33 Vispe S, DeVries L, Creancier L, Besse J, Breand S, Hobson DJ, Svejstrup JQ, Annereau JP, Cussac D, Dumontet C, Guilbaud N, Barret JM, Bailly C: Triptolide is an inhibitor of RNA polymerase I and II-dependent transcription leading predominantly to down-regulation of short-lived mRNA. Mol Cancer Ther 2009;8:2780-2790.
34 da Costa JP, Carvalhais V, Ferreira R, Amado F, Vilanova M, Cerca N, Vitorino R: Proteome signatures-how are they obtained and what do they teach us? Applied Microbiology and Biotechnology 2015;99:7417-7431.
35 Pe'er D, Hacohen N: Principles and strategies for developing network models in cancer. Cell 2011;144:864-873.
36 Bonnal S, Vigevani L, Valcarcel J: The spliceosome as a target of novel antitumour drugs. Nat Rev Drug Discov 2012;11:847-859.
37 Sato N, Maeda M, Sugiyama M, Ito S, Hyodo T, Masuda A, Tsunoda N, Kokuryo T, Hamaguchi M, Nagino M, Senga T: Inhibition of SNW1 association with spliceosomal proteins promotes apoptosis in breast cancer cells. Cancer Med 2015;4:268-277.
38 Kim MJ, Lee TH, Kim SH, Choi YJ, Heo J, Kim YH: Triptolide inactivates Akt and induces caspase-dependent death in cervical cancer cells via the mitochondrial pathway. Int J Oncol 2010;37:1177-1185.
39 Xie CQ, Zhou P, Zuo J, Li X, Chen Y, Chen JW: Triptolide exerts pro-apoptotic and cell cycle arrest activity on drug-resistant human lung cancer A549/Taxol cells via modulation of MAPK and PI3K/Akt signaling pathways. Oncol Lett 2016;12:3586-3590.
40 Chan CC, Dostie J, Diem MD, Feng W, Mann M, Rappsilber J, Dreyfuss G: eIF4A3 is a novel component of the exon junction complex. RNA 2004;10:200-209.
41 Quaresma AJ, Sievert R, Nickerson JA: Regulation of mRNA export by the PI3 kinase/AKT signal transduction pathway. Mol Biol Cell 2013;24:1208-1221.
42 Zhou Z, Luo MJ, Straesser K, Katahira J, Hurt E, Reed R: The protein Aly links pre-messenger-RNA splicing to nuclear export in metazoans. Nature 2000;407:401-405.
43 Okada M, Jang SW, Ye K: Akt phosphorylation and nuclear phosphoinositide association mediate mRNA export and cell proliferation activities by ALY. Proc Natl Acad Sci U S A 2008;105:8649-8654.
44 Stubbs SH, Conrad NK: Depletion of REF/Aly alters gene expression and reduces RNA polymerase II occupancy. Nucleic Acids Res 2015;43:504-519.
45 Fuentes JL, Datta K, Sullivan SM, Walker A, Maddock JR: *In vivo* functional characterization of the Saccharomyces cerevisiae 60S biogenesis GTPase Nog1. Mol Genet Genomics 2007;278:105-123.
46 Yu H, Jin S, Zhang N, Xu Q: Up-regulation of GTPBP4 in colorectal carcinoma is responsible for tumor metastasis. Biochem Biophys Res Commun 2016;480:48-54.

47 Hu ZW, Shi XY, Lin RZ, Hoffman BB: Contrasting signaling pathways of alpha1A- and alpha1B-adrenergic receptor subtype activation of phosphatidylinositol 3-kinase and Ras in transfected NIH3T3 cells. Mol Endocrinol 1999;13:3-14.
48 Uberall F, Hellbert K, Kampfer S, Maly K, Villunger A, Spitaler M, Mwanjewe J, Baier-Bitterlich G, Baier G, Grunicke HH: Evidence that atypical protein kinase C-lambda and atypical protein kinase C-zeta participate in Ras-mediated reorganization of the F-actin cytoskeleton. J Cell Biol 1999;144:413-425.
49 Lunardi A, Di Minin G, Provero P, Dal Ferro M, Carotti M, Del Sal G, Collavin L: A genome-scale protein interaction profile of Drosophila p53 uncovers additional nodes of the human p53 network. Proc Natl Acad Sci U S A 2010;107:6322-6327.
50 Peng YT, Chen P, Ouyang RY, Song L: Multifaceted role of prohibitin in cell survival and apoptosis. Apoptosis 2015;20:1135-1149.
51 Cimadamore F, Curchoe CL, Alderson N, Scott F, Salvesen G, Terskikh AV: Nicotinamide rescues human embryonic stem cell-derived neuroectoderm from parthanatic cell death. Stem Cells 2009;27:1772-1781.
52 Hong SJ, Dawson TM, Dawson VL: Nuclear and mitochondrial conversations in cell death: PARP-1 and AIF signaling. Trends Pharmacol Sci 2004;25:259-264.
53 Yu SW, Andrabi SA, Wang H, Kim NS, Poirier GG, Dawson TM, Dawson VL: Apoptosis-inducing factor mediates poly(ADP-ribose) (PAR) polymer-induced cell death. Proc Natl Acad Sci U S A 2006;103:18314-18319.
54 Dang NH, Singla AK, Mackay EM, Jirik FR, Weljie AM: Targeted cancer therapeutics: biosynthetic and energetic pathways characterized by metabolomics and the interplay with key cancer regulatory factors. Curr Pharm Des 2014;20:2637-2647.
55 Masoudi-Nejad A, Asgari Y: Metabolic cancer biology: structural-based analysis of cancer as a metabolic disease, new sights and opportunities for disease treatment. Semin Cancer Biol 2015;30:21-29.
56 Fulda S, Galluzzi L, Kroemer G: Targeting mitochondria for cancer therapy. Nat Rev Drug Discov 2010;9:447-464.
57 Yang S, Chen J, Guo Z, Xu XM, Wang L, Pei XF, Yang J, Underhill CB, Zhang L: Triptolide inhibits the growth and metastasis of solid tumors. Mol Cancer Ther 2003;2:65-72.
58 Sangwan V, Banerjee S, Jensen KM, Chen Z, Chugh R, Dudeja V, Vickers SM, Saluja AK: Primary and liver metastasis-derived cell lines from KrasG12D; Trp53R172H; Pdx-1 Cre animals undergo apoptosis in response to triptolide. Pancreas 2015;44:583-589.
59 Covington KR, Fuqua SA: Role of MTA2 in human cancer. Cancer Metastasis Rev 2014;33:921-928.
60 Zhou C, Ji J, Cai Q, Shi M, Chen X, Yu Y, Liu B, Zhu Z, Zhang J: MTA2 promotes gastric cancer cells invasion and is transcriptionally regulated by Sp1. Mol Cancer 2013;12:102.
61 Vergara D, Simeone P, Latorre D, Cascione F, Leporatti S, Trerotola M, Giudetti AM, Capobianco L, Lunetti P, Rizzello A, Rinaldi R, Alberti S, Maffia M: Proteomics analysis of E-cadherin knockdown in epithelial breast cancer cells. J Biotechnol 2015;202:3-11.
62 Pannone G, Santoro A, Feola A, Bufo P, Papagerakis P, Lo Muzio L, Staibano S, Ionna F, Longo F, Franco R, Aquino G, Contaldo M, De Maria S, Serpico R, De Rosa A, Rubini C, Papagerakis S, Giovane A, Tombolini V, Giordano A, Caraglia M, Di Domenico M: The role of E-cadherin down-regulation in oral cancer: CDH1 gene expression and epigenetic blockage. Curr Cancer Drug Targets 2014;14:115-127.
63 Mareel MM, Behrens J, Birchmeier W, De Bruyne GK, Vleminckx K, Hoogewijs A, Fiers WC, Van Roy FM: Down-regulation of E-cadherin expression in Madin Darby canine kidney (MDCK) cells inside tumors of nude mice. Int J Cancer 1991;47:922-928.
64 Zhang B, Zhang H, Shen G: Metastasis-associated protein 2 (MTA2) promotes the metastasis of non-small-cell lung cancer through the inhibition of the cell adhesion molecule Ep-CAM and E-cadherin. Jpn J Clin Oncol 2015;45:755-766.